

Supplementary Information

Impermeable Atomic Membranes from Graphene Sheets

J. Scott Bunch, Scott S. Verbridge, Jonathan S. Alden, Arend M. van der Zande, Jeevak M. Parpia,

Harold G. Craighead, Paul L. McEuen

Cornell Center for Materials Research, Cornell University, Ithaca NY 14853

Experimental Methods

Graphene drumheads are fabricated by a combination of standard photolithography and mechanical exfoliation of graphene sheets. First, a series of squares with areas of 1 to 100 μm^2 are defined by photolithography on an oxidized silicon wafer with a silicon oxide thickness of 285 nm or 440 nm. Reactive ion etching is then used to etch the squares to a depth of 250 nm to 3 μm leaving a series of wells on the wafer. Mechanical exfoliation of Kish graphite using Scotch tape is then used to deposit suspended graphene sheets over the wells.

To determine the elastic constants of graphene using equation (3), we extrapolate the deflection in Fig. 1e (inset) to $z = 181$ nm to account for a 40-minute sample-load time, assume an initial pressure difference across the membrane, $\Delta p = 93$ kPa, and a negligible initial tension. The latter two assumptions are verified using resonance measurements. The actual deflection used in equation (3) is obtained by subtracting the extrapolated deflection $z = 181$ nm from the initial deflection $z_0 = 23 \pm 3$ nm at $\Delta p = 0$. This initial deflection is determined from the AFM image in Fig. 4a and AFM force-distance curves Fig. S1.

Slack and Self Tensioning at $\Delta p = 0$

Since the cantilever-surface interaction is expected to be different for AFM measurements over the relatively-pliable suspended and the rigid SiO₂-supported graphene, the depth of the membrane z_0 , at $\Delta p = 0$ must be determined via force and amplitude calibrations of the cantilever over each surface (Whittaker, Minot et al. 2006). A representative calibration measurement is shown in Fig. S.1. Both the amplitude (upper) and deflection (lower) of the AFM tip is measured while approaching the surface.

Over the SiO₂-supported surface, the difference between the actual surface position and the position given by the image in Fig. 4a can be determined by subtracting the height at which the AFM tip begins to bend due to unbroken contact with the surface (A) from the height at which the amplitude setpoint intersects with the amplitude response curve (B) (Fig. S.1). The surface is determined to be 30 nm below the amplitude setpoint position.

Since suspended graphene is more pliable than supported graphene, the onset of the AFM cantilever's deflection of Fig. S.1 is more gradual, and thus cannot be readily used to determine the equilibrium height of the suspended graphene. Instead, we note that when in unbroken-contact with the graphene surface, any deviations of the AFM tip from the equilibrium (lowest-strain) depth of the membrane will result in an increase in the membrane tension as the tip either pulls up or pushes down on the membrane. This increase in tension on either side of the equilibrium position will cause a decrease in cantilever response amplitude, resulting in a peak in the cantilever-amplitude response at the equilibrium position, similar to what has been observed for suspended carbon nanotubes (Whittaker, Minot et al. 2006). This occurs at ~100 nm, or 34 nm below the amplitude setpoint position (C).

Comparing these setpoint-to-surface depths for suspended and supported graphene, we find that the equilibrium depth of the suspended membrane is $17 + (34 - 30) = 21$ nm below the SiO₂-supported surface where 17 nm is the distance measured in Fig. 4a. Repeating these measurements across the

center of the membrane yields an average equilibrium membrane-depth $z_0 = 17 \pm 1 \text{ nm} + (6 \pm 2 \text{ nm}) = 23 \pm 3 \text{ nm}$.

Measuring the Gas Leak Rates

The gas leak rate is measured by monitoring the internal pressure, p_{int} , vs. time. For the case of the leak rate of air, the microchamber begins with $p_{int} \sim 100 \text{ kPa}$ Air. This is verified by a scan of frequency vs. p_{ext} , as in Fig. 3. A similar scan is performed once every few hours to monitor p_{int} while the device is left at $p_{ext} \sim 0.1 \text{ mPa}$ between each measurement (Fig. 3a and 3b). The leak rate of argon is measured in a similar manner except the microchamber begins with a $p_{int} \sim 0 \text{ kPa}$ argon and $\sim 10 \text{ kPa}$ air. The microchamber is left in $p_{ext} \sim 100 \text{ kPa}$ argon between measurements to allow argon to diffuse into the microchamber. This diffusion is monitored by finding the minimum pressure in a scan of frequency vs. p_{ext} .

To measure the helium leak rate we apply a $\Delta p \sim 40 - 50 \text{ kPa}$ He and monitor the resonance frequency as helium diffuses into the microchamber. It will diffuse until the partial pressure of helium is the same inside and outside the microchamber (Fig. S2). From the slope of the line we extract a helium leak rate for the devices using equation (1). Leak rates from square membranes with sides varying from 2.5 to 4.8 μm were measured with no noticeable dependence of the leak rate on area.

Transmission Probability

Using this measured leak rate, we estimate an upper bound for the average transmission probability of a He atom impinging on a graphene surface as:

$$\frac{dN}{dt} \frac{2d}{Nv} < 10^{-11} \quad (\text{S.1})$$

where dN/dt is the measured leak rate, d is the depth of the microchamber, and v is the velocity of He atoms. The number of He atoms/second impinging on the graphene seal is given by $\sim Nv/2d$, since each atom takes a time $\sim 2d/v$ to make a round trip in the chamber. Dividing the measured rate by this value,

gives us the upper bound estimate given above in (S.1).

Tunneling of He Atoms across a Graphene Sheet

In the WKB approximation of tunneling probability, the probability of a particle with a mass m , tunneling across a finite potential barrier with a height V , and distance x , is given by:

$$p = e^{\frac{-2x\sqrt{2m(V-E)}}{\hbar}} \quad (S.2)$$

To estimate tunneling through a perfect graphene sheet with $E \sim 25$ meV, we assume a barrier has $V \sim 8.7$ eV and a thickness $x \sim 0.3$ nm. This gives a tunneling probability $p \sim 1 \times 10^{-335}$. For the case of tunneling through a “window” mechanism whereby temporary bond breaking lowers the barrier height to ~ 3.5 eV, the tunneling probability at room temperature is $p \sim 1 \times 10^{-212}$ which is still many orders of magnitude smaller than we observe (Hrusak, Bohme et al. 1992; Saunders, Jimenez-Vazquez et al. 1993; Murry and Scuseria 1994).

Classical Effusion through Single Atom Lattice Vacancies

For the case of classical effusion out of a container with a small hole, the number of molecules inside the container is given by:

$$n = n_0 e^{-\frac{A}{V} \sqrt{\frac{k_b T}{2\pi m}} t} \quad (S.3)$$

where n_0 is the initial number of molecules, A is the area of the hole, V is the volume of the container, k_b is Boltzman’s constant, T is temperature, t is time, and m is the atomic mass of the gas (Reif 1965). For a defect area of 1 nm^2 , effusion of gas would take place in much less than one second. Even a one atom defect would leak in less than one second.

The reason for such fast effusion is the volume of the container for the graphene sealed

microchambers is so small (typically $\sim 1 \mu\text{m}^3$). The number of molecules in the microchamber depends on the ratio A/V , and a defect with an area of 1 nm^2 in a $1 \mu\text{m}^3$ box yields an area/volume ratio of 1 m^{-1} . If this was scaled up to macroscopic dimensions, it is equivalent to a 1 m^3 box with a defect of area = 1 m^2 . This suggests that any leak rate out of nanochambers is extremely sensitive to the defect area and therefore an accurate measure of that area. This makes detection of small changes in defect area by adsorbed molecules highly sensitive. One should note that such a detection scheme is impossible with thicker silicon NEMS since their compliance seriously diminishes when the lateral dimensions approach $1 \mu\text{m}$. By using atomic scale thickness resonators, we can overcome these inherent limitations in Si MEMS technology. Previous attempts to fabricate compliant micron size membranes have focused on nanoparticle arrays and inorganic membranes (Jiang, Markutsya et al. 2004; Mueggenburg, Lin et al. 2007). Our graphene membranes are 30-100 times thinner and have a single crystal structure making them much more robust.

Supplementary References:

Jiang, C., S. Markutsya, et al. (2004). "Freely suspended nanocomposite membranes as highly sensitive sensors." Nat Mater **3**(10): 721-728.

Mueggenburg, K. E., X.-M. Lin, et al. (2007). "Elastic membranes of close-packed nanoparticle arrays." Nat Mater **6**(9): 656-660.

Reif, F. (1965). Fundamentals of Statistical and Thermal Physics. New York, NY, McGraw-Hill Book Company.

Whittaker, J. D., E. D. Minot, et al. (2006). "Measurement of the Adhesion Force between Carbon Nanotubes and a Silicon Dioxide Substrate." Nano Lett. **6**(5): 953-957.

Figure S1

(upper) Driven oscillation amplitude of the tapping mode AFM cantilever with resonance frequency = 349 kHz vs. piezo extension as tip is brought into contact with the surface. Black and red are extension and retraction curves over the supported graphene on SiO₂ surface. Green and blue are extension and retraction curves over the suspended graphene membrane. (lower) The deflection of the cantilever vs. piezo extension. The upper and lower traces were taken simultaneously.

Figure S2

Resonance frequency vs. time for a single layer graphene sealed nanochamber exposed to 357 torr external pressure of He. The internal pressure of the nanochamber is initially at 500 torr of Air. At time $t = 0$ sec, 357 torr external pressure of He is applied to the nanochamber. The resonant frequency is measured every few seconds until the frequency approaches its initial value.

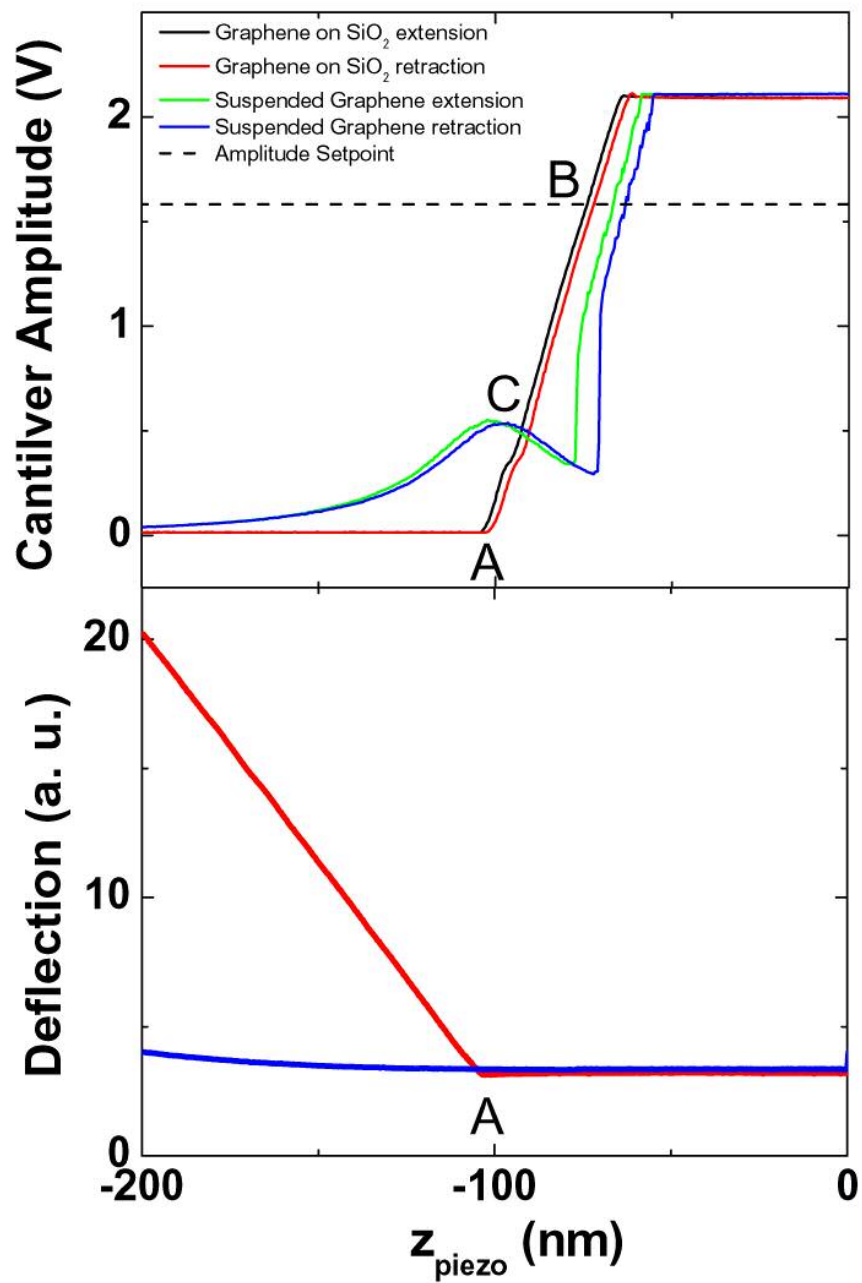


Fig. S1

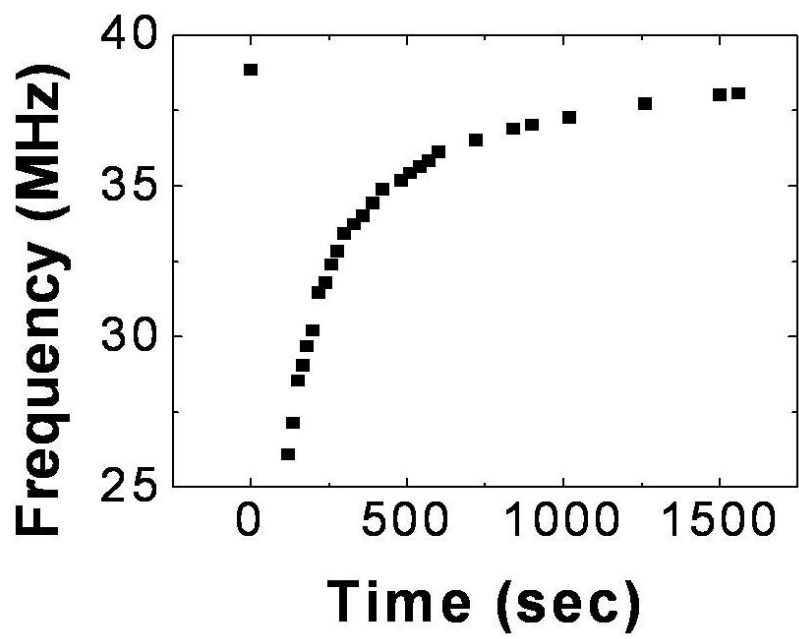


Fig. S2